Astron. Astrophys. 364, 282–292 (2000)

ASTRONOMY AND ASTROPHYSICS

Steps toward interstellar silicate mineralogy

V. Thermal evolution of amorphous magnesium silicates and silica

D. Fabian, C. Jäger, Th. Henning, J. Dorschner, and H. Mutschke

University of Jena, Astrophysical Institute and University Observatory (AIU), Schillergässchen 3, 07745 Jena, Germany

Received 17 December 1999 / Accepted 26 April 2000

Abstract. The thermally induced amorphous-to-crystalline transition has been studied for bulk sheets and micrometre-sized particles of magnesium silicate glass ($MgSiO_3$), nanometre-sized amorphous magnesium silicate ($MgSiO_3$ and Mg_2SiO_4 smokes) and amorphous silica particles (SiO_2). Silicate glass was produced by the shock-quenching of melts. Samples of nanometre-sized smoke particles have been obtained by the laser ablation technique.

Both the $MgSiO_3$ and the Mg_2SiO_4 smokes have been found to consist of two particle species; particles of smaller size ranging in diametre from 10 nm to about 100 nm and bigger size ranging from a few 100 nm to almost 3 micrometres in diametre. Nanometre-sized particles have been shown to be depleted in magnesium whereas the micrometre-sized particles were found to be enriched in Mg. Generally, the particles are composed of nonstoichiometric magnesium silicates with compositions varying even inside of the particles. Frequently, the particles contained internal voids that are assumed to have been formed by thermal shrinkage or outgassing of the particles' interior during cooling.

Annealing at 1000 K transformed the magnesium silicate smokes into crystalline forsterite (c-Mg_2SiO_4), tridymite (a crystalline modification of SiO_2) and amorphous silica (a-SiO_2) according to the initial Mg/Si-ratio of the smoke. Crystallization took place within a few hours for the Mg_2SiO_4 smoke and within one day for the $MgSiO_3$ smoke.

The $MgSiO_3$ glass evolved more slowly because crystallization started at the sample surface. It has been annealed at temperatures ranging from 1000 to 1165 K. In contrast to the smoke samples, $MgSiO_3$ glass crystallized as orthoenstatite ($MgSiO_3$). Only after 50 hours of annealing at 1000 K, weak indications of forsterite and tridymite formation have been found in the X-ray diffraction spectra.

At a temperature of 1000 K, amorphous silica nanoparticles showed distinctly lower rates of thermal evolution compared with the magnesium silicates. At 1220 K, the timescale of crystallization of a-SiO_2 into cristobalite and tridymite amounts to 4.5 h.

From the experiments, crystallization parameters have been obtained: activation energy and velocity of crystal growth.

The spectra shown in this study will be made publically available in the electronic database (http://www.astro.uni-jena.de).

Key words: stars: circumstellar matter – stars: formation – stars: AGB and post-AGB – solar system: formation – methods: laboratory

Send offprint requests to: D. Fabian (fabian@astro.uni-jena.de)

1. Introduction

The Infrared Space Observatory (ISO) has opened the mid- and far-infrared range for high-resolution spectroscopy and provided striking evidence for the presence of crystalline Mg-rich silicates in comets (Crovisier et al. 1997), circumstellar regions (envelopes/disks) around young stars (Waelkens et al. 1998; Malfait et al. 1999) and evolved stars (Waters et al. 1996; Molster et al. 1998, 1999a). In contrast to chaotic silicates (Nuth 1996) and silicate glasses (Jäger et al. 1994; Dorschner et al. 1995; Mutschke et al. 1998), crystalline silicates show a lot of diagnostic bands due to metal-oxygen vibrations which can be used to identify the minerals of cosmic silicates (Jäger et al. 1998; Koike et al. 1993).

In terrestrial environments, crystalline silicates are mainly formed from cooling melts, from aqueous solutions or by hydrothermal alteration of anhydrous silicates. In astrophysical environments, as listed below, crystalline silicates evolve from amorphous low-pressure condensates by the process of annealing that is characterized by the formation of an ordered arrangement of the silicate tetrahedra by thermal atomic diffusion. In the tetrahedral units themselves, only minor changes occur (Thompson et al. 1996). The crystalline phases developing from amorphous magnesium silicates and from silica are given explicitly (see Table 1).

The annealing process may well happen in the envelopes around AGB stars (Gail & Sedlmayr 1998; Sogawa & Kozasa 1999; Gail & Henning 1999) and therefore deserves great attention in astrophysical context.

Table 1. Developing crystalline phases and some properties

Mineral	Formula	Structure
enstatite	$MgSiO_3$	pyroxen, rhombic
forsterite	Mg_2SiO_4	olivine, rhombic
tridymite and	SiO_2	high-temperat. mod.
cristobalite		$T > 1143K$

During annealing, thermal diffusion finally leads to a rearrangement of the structural units producing long-range order. Diffusion in solids is based on lattice defects that are thermally activated. That means that thermal diffusion and crystallization can also be stimulated by irradiation and OH enrichment of the silicates. The formation of defects can be non-thermally triggered by particle irradiation ('enhanced diffusion', Frank et al. 1979). OH anions incorporated in silicates reduce the viscosity and promote crystallization and phase separation (Scholze 1988). In low-temperature environments such as molecular clouds, a long-duration exposure to cosmic rays may lead to an accumulation of defects. Thus, the structure of such silicate particles might be characterized by a predominantly non-thermal defect concentration. If a cloud core collapses to form a new star, the dust particles are subjected to temperature rises. The non-thermal defect concentration inherited from the irradiation prehistory might enhance diffusion and promote crystallization. Laboratory experiments have shown that amorphous SiO can crystallize under 80 keV He^+ bombardment (Walters et al. 1988). The material was heated up to 1120 K during ion bombardment. At this temperature, the non-irradiated samples did not show crystallization.

In cold dust environments (the dust shell around the young Fe star HD 142527 and comet Hale Bopp) partially crystalline silicates have been recently observed that may have been formed by crystallization at low temperature. In the spectrum of HD 142527, indications have been found that cold crystalline silicates are associated with hydrous silicates (Malfait et al. 1999; Wooden et al. 1999; Molster et al. 1999b). Laboratory experiments confirmed that Mg-SiO smokes are transformed into protophyllosilicates by low-temperature annealing in the presence of H_2O. This way, Rietmeijer (1995) demonstrated that Mg-SiO smoke was transformed to saponite and talc by annealing at 378 K after 7.5 h.

In this paper, the differences in the thermal evolution of nanometre-sized magnesium silicate smokes and silica on the one hand and glassy micrometre-sized and bulk magnesium silicates on the other hand will be outlined.

Glassy silicates have a homogeneous chemical composition compared to smokes. From infrared (IR) spectroscopy and transmission electron microscopy (TEM), kinetic constants of the annealing process have been obtained. Silica has been studied as an appearing component during annealing of magnesium smoke and as pure silica; rather different timescales of crystallization have been observed. Additionally, in the far infrared wavenumber range, an opacity drop due to crystallization has been studied.

During annealing at 1000 K up to 4 h, Rietmeijer et al. (1986) found that enstatite crystals had evolved from previously formed tridymite and forsterite nanocrystals. In the study by Hallenbeck et al. (1998), enstatite has not been observed after annealing times up to 3 h at 1200 K. These results have to be compared with the evolution of glassy silicates studied in this paper.

Using IR spectroscopy, Hallenbeck et al. (1998) monitored a "stall" phase, in which the spectra remained almost unaltered. But it remained unclear, why this stall phase occurred and if a stall would occur during annealing of glassy magnesium silicates (Rietmeijer et al. 1986; Hallenbeck et al. 1998). We will deal with this issue.

2. Observational evidence for crystalline silicates in space

As a basis for the experimental strategy of this paper, we will summarize the overwhelming evidence for the presence of crystalline silicates in space.

2.1. Meteorites

Primitive meteorites present convincing evidence concerning the origin of the solar system. Starting from a fine-grained crystalline or amorphous precursor material, the matrix of carbonaceous chondrites has most probably suffered from a thermal evolution influenced by hydrous alteration (Taylor 1992; Brearley 1996). Low-temperature annealing ($T < 1000\,\mathrm{K}$) appears to be the most likely mechanism to reproduce the features of the matrix. Later, the texture and stoichiometry has been changed by aqueous alteration and thermal metamorphism of the meteorite parent body (Kojima & Tomeoka 1996).

Apart from nanometre-sized particles, amorphous bulk material should be present in protoplanetary accretion disks. The prominent objects in chondrites, olivine-pyroxene chondrules that have typical diametres of about 0.5 to 1.5 mm, appear to have crystallized from flashlike molten or partly molten drops (Taylor 1992). Hence, the overall kinetics of bulk crystallization has to be investigated experimentally.

2.2. IDPs and cometary grains

Comets, such as C/1995 O1 (Hale Bopp), are frozen reservoirs of primitive materials from the early solar system and represent a major source for interplanetary dust particles (IDPs) (Sandford 1996; Crovisier et al. 1997; Bradley et al. 1999b). These chondritic porous IDPs contain submicrometre-sized forsterite, enstatite and glassy silicate grains. The glassy silicates are also called GEMS (glass with embedded metal and sulfides). The structural and optical properties of the GEMS are similar to those expected for interstellar silicates and their structure suggests a pre-accretional origin (Bradley et al. 1999a).

Both carbonaceous *and* silicatic features are present in cometary spectra. In detail, the mid-IR emission spectra of comet P/Halley imply that Mg-rich crystalline olivines are a major mineral component of the inner coma. In addition to crys-

talline olivines, amorphous Mg-silicates are present in cometary dust (Hanner 1999).

Crystalline silicates in cometary dust have been probably formed by the process of annealing. If stimulation by irradiation and OH-enrichment would not be sufficient to promote crystallization at low temperatures, this fact would imply that solar system formation must have been accompanied by large-scale radial mixing of condensates from the hot terrestrial planet zones to the icy planetesimal zones beyond Jupiter's orbit (Wooden et al. 1999).

2.3. Circumstellar environment around young stars

Amorphous silicates with composition and structure inherited from the parent molecular cloud enter an accretion disk and move slowly inwards. Proceeding to layers of sufficiently high temperature, diffusion and crystallization processes start. At different material-dependent timescales, the amorphous structure is converted into an ordered lattice structure.

In detail, in the shell surrounding the isolated Fe star HD 142527, a warm (500 to 1500 K) and a cold (30 to 60 K) dust component could be distinguished. The cold dust is mainly composed of partially crystalline silicates. Surprisingly, crystalline silicates have not been observed in the warm dust environment (Malfait et al. 1999). As was already noted in the preceding section, crystallization of silicates in cold environments might have been stimulated by irradiation or OH-enrichment. The importance of low-temperature crystallization processes has been outlined recently by Molster et al. (1999b).

Modelling of a thin steady-state protoplanetary accretion disk with a central stellar mass of $1\ \mathrm{M}_\odot$ and an accretion rate of $10^{-7}\mathrm{M}_\odot\mathrm{yr}^{-1}$ showed that crystallization of the dirty silicate dust starts at about 800 K at a radial distance from the star of 2...1 AU (Gail 1998).

2.4. AGB and Post-AGB stars

In the AGB stage, stars are cool ($T_{\rm eff} = 2000 - 2500$ K), luminous ($L = 10^4\,L_\odot$) and extended ($R_\star = 10^3\,R_\odot$) red giants. Their mass loss rates range between less than $10^{-7}\mathrm{M}_\odot\mathrm{yr}^{-1}$ and more than $10^{-4}\,\mathrm{M}_\odot\mathrm{yr}^{-1}$. The central stars are usually obscured by their dusty envelopes. They are detected by the infrared emission from their expanding dust shells. The expansion velocity is in the range from 10 to 25 km s^{-1}. AGB stars are an important dust source injecting newly formed grains into interstellar space ("stardust"). In stars of spectral type M, the oxygen abundance exceeds that of carbon. Hence, M-stars mainly form silicate dust. For reasons of elemental abundance, it is generally believed that the dominating dust condensates are olivine and pyroxene (Dorschner & Henning 1995; Henning 1999).

Silicate condensation may start at a temperature of 1000 K or slightly lower on some preexisting nuclei (e.g. $\mathrm{TiO_x}$ clusters). Silicates should be amorphous at the initial stage of condensation. During the process of annealing, an ordered structure can develop. An at least partially crystalline structure would be established if the cooling rate of the outflow were comparable to the typical annealing time (Gail & Sedlmayr 1998; Gail & Henning 1999).

3. Basic parameters of crystallization

At sufficiently high temperatures, the atoms in a poorly ordered dust material start to rearrange and to migrate into energetically more favorable positions, i.e. the dust material's structure gradually changes into the topology of a microcrystalline material. Even mass-dependent fractionation can occur. In systems that tend to decompose, chemical fractionation takes place.

Crystallization is a complicated process usually including nucleation and crystal growth. A comprehensive description of crystallization has to be based on a detailed kinetic theory (Vogel 1985; Gutzow & Schmelzer 1995).

We use an empirical approach for the description of this process that statistically includes both nucleation and crystal growth. In this approach, the overall crystallization is related to the spectroscopic behaviour of the samples. A characteristic annealing time τ can be defined as the time of the appearance of an ordered structure usually monitored by IR spectroscopy and X-ray diffraction (XRD) analyses. Its value can be expressed by

$$\tau^{-1} = \nu_0 e^{-E_{\rm a}/kT}, \tag{1}$$

where $E_{\rm a}$ is the effective activation energy empirically comprising nucleation and crystallization energy. The quantity ν_0 is a constant that is proportional to the mean vibrational frequency of the silicate lattice (Lenzuni et al. 1995). For magnesium silicates, the mean vibrational frequency of the lattice is $2.0 \times 10^{13}\,\mathrm{s}^{-1}$ (Gail & Sedlmayr 1998). In the first place, we set ν_0 to this value and keep in mind that the value of the activation energy derived from Eq. (1) depends on the value chosen for ν_0. Furthermore, we define a diffusion constant D and a unit of size l of already established crystalline order after a time t. They are related by the following equations (Gail & Sedlmayr 1998):

$$l^2 = 6D(T)t \tag{2}$$

$$D = \frac{a^2\nu_0}{3} e^{-E_{\rm a}/kT} \tag{3}$$

with a as the characteristic lattice length. In this paper, the activation energy is determined from annealing time measurements using Eq. (1).

As will be outlined in the following section, the overall crystallization of amorphous materials is associated with a significant drop in opacity in the far infrared (FIR) and a sharpening of absorption features in the mid infrared spectral range (MIR) (Henning et al. 1995). In the FIR, the dependence of the mass absorption coefficient on the wavelength can often be approximated by a power law

$$\kappa = \kappa_0 \left(\frac{\nu}{\nu_1}\right)^\beta, \tag{4}$$

where β is the spectral index and $\kappa_0 = \kappa(\nu_1)$ with $\nu_1 = 1\,\mathrm{cm}^{-1}$. Eq. (4) has been applied to evaluate the FIR absorption of smoke-like and powder samples.

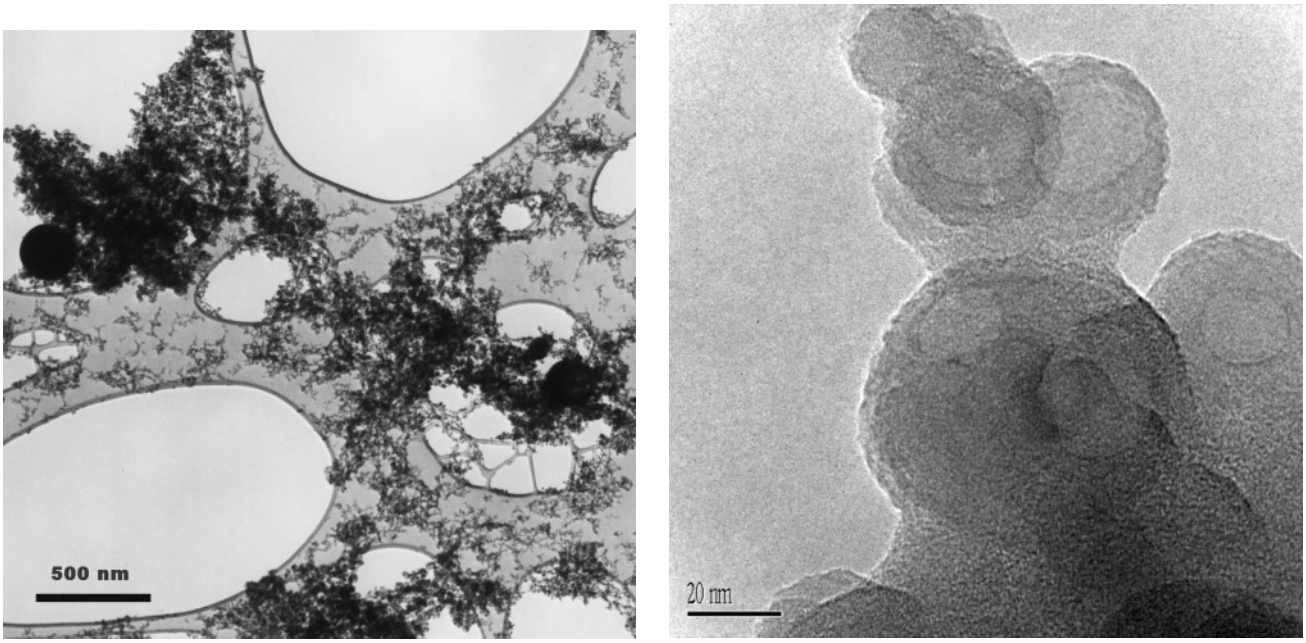

Fig. 1. TEM images of laser-ablated $MgSiO_3$ smoke. Spherical micrometre- and nanometre-sized smoke particles are composed of nonstoichiometric Mg-silicates. In the particles with diametres ranging from 10 to 50 nm, voids are contained frequently.

4. Experimental

4.1. Preparation and sample characterization

For the annealing experiments, amorphous silicate materials have to be produced. The following methods for their production have been applied:

4.1.1. Magnesium silicate glass ($MgSiO_3$)

Silicate melts have been produced from a mixture of magnesium carbonate and silica powder in enstatite stoichiometry. The melts were shock-quenched ($\approx$ 1000 K/s) by pouring the melt through spinning copper rollers. Glassy sheets were obtained of about 100 to 130 μm thickness. The samples did not show any indications for phase separation or crystalline nucleation.

For powder experiments, the sheets were ground to irregularly shaped particles of about 5 to 10 μm diameter. Detailed studies of glassy silicate materials have already been published in preceding papers and will not be repeated here (Jäger et al. 1994; Dorschner et al. 1995; Mutschke et al. 1998; Jäger et al. 1998). Glassy Mg-silicates have been considered as a reliable approximation expected for the grain material in space. In IDP's and cometary grains, primitive silicate glass grains (GEMS) of assumed preaccretional origin also occur (Bradley 1994; Bradley et al. 1999a).

4.1.2. Nanometre-sized particles ($MgSiO_3$ and Mg_2SiO_4 smoke)

Amorphous magnesium silicate smokes were obtained by laser ablation of $MgSiO_3$ and Mg_2SiO_4 targets in 1 atm oxygen atmosphere (Nd:YAG-laser, 6 J/pulse, wavelength 1064 nm).

Using a Jeol 300 kV transmission electron microscope, two differently-sized smoke particle species have been observed in both the $MgSiO_3$ and the Mg_2SiO_4 smoke. The smaller species, about 10 to 50 nm in diametre, had been remarkably magnesium deficient. In the case of the $MgSiO_3$ smoke, their composition had been close to SiO_2. In the Mg_2SiO_4 smoke, the particles showed a Mg/Si ratio ranging from at least 0.5 to 1. In contrast, the second particle species ranging in size from 0.1 to 2 μm has been found to be rich in magnesium. The chemical composition of the biggest ones, about 1 to 2 micrometres in size, had been close to that of the ablated target, i.e. the Mg/Si ratio was 1 for the $MgSiO_3$ and 2 for the Mg_2SiO_4 smoke. Generally, the smoke particles consisted of a mixture of rather nonstoichiometric magnesium silicates varying from particle to particle and even inside the particles. Weak absorption features that can be observed in the MIR spectra of both smokes indicate that some forsterite microcrystallites have formed in the predominantly amorphous smoke particles during the laser ablation process (see Fig. 5 and 7). Independent of the size, the particle shapes were nearly spherical indicating that the particles have most probably experienced a melting phase.

As a frequent characteristic property, most of the particles contained voids that are assumed to have formed by outgassing and by contraction of the originally molten droplets. Formation of voids can also be triggered during observation in the TEM, indicating that a certain amount of gas is still trapped in the amorphous structure and can be released by irradiation (see Fig. 1).

4.2. Annealing experiments

The annealing experiments with glassy and smoke-like silicates have been performed in a Nabertherm HT 04/17 oven in an

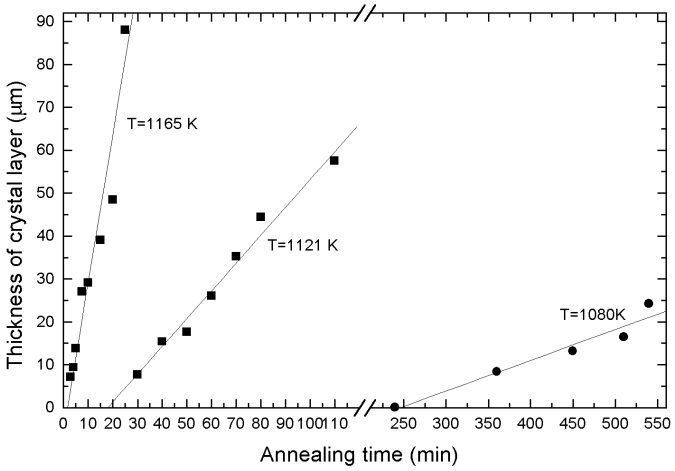

Fig. 2. Thickness growth of the orthoenstatite layer on a sheet of $MgSiO_3$ glass with increasing annealing time for different temperatures.

Table 2. Kinetic data of crystallization of bulk $MgSiO_3$ glass

Temperature (K)	Growth rate v_c (μm/min)	Time-lag (min)
1165	3.46	1.6
1121	0.65	18
1080	0.072	246

oxygen atmosphere of 1 atm to prevent evaporative magnesium loss that was observed during annealing in vacuum (Rietmeijer et al. 1986; Karner & Rietmeijer 1996; Hallenbeck et al. 1998).

From the annealed samples of powders embedded in KBr and polyethylene (PE) pellets, IR transmission spectra have been obtained. A Bruker IFS 113 FTIR spectrometer has been used.

4.2.1. Bulk and micrometre-sized $MgSiO_3$ glass

Glassy sheets have been annealed as a bulk material at temperatures of 1165, 1121 and 1080 K. The surface evolution was monitored by scanning electron microscopy (SEM) and IR spectroscopy.

Heterogeneous nucleation and crystallization started at the sheet's surface to create a growing orthoenstatite layer. The layer thickness was measured by SEM of the cross section after thermal treatment. To derive kinetic constants, the layer's thickness was measured as a function of annealing time (see Fig. 2). Additionally, time-lag effects of nucleation were observed before crystal growth started. The velocity of linear crystal growth v_c was calculated from the layer thickness (see Table 2). Its values correspond well to the annealing times that have been obtained for powdered glass as will be outlined below.

For small particles, shorter annealing times are expected compared with the time for the bulk samples because of the strongly increased particle surface. To investigate the thermal evolution of such small particles, the bulk glass sheets have been ground using an agate mill.

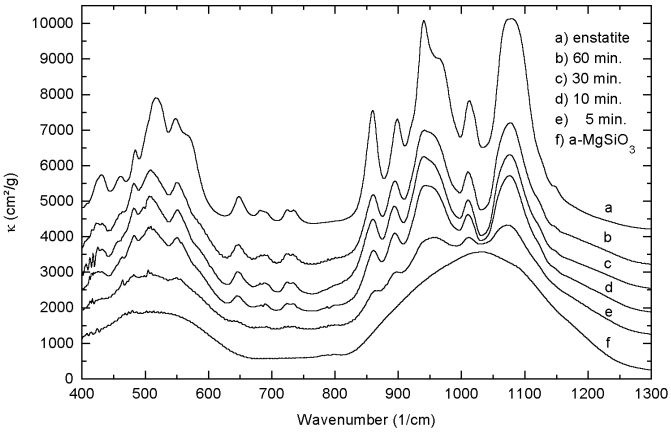

Fig. 3. Evolution of the MIR spectrum of $MgSiO_3$ glass particles (f). At T=1121 K, the annealing times for the spectra are indicated. For comparison, the enstatite spectrum (a, from Jäger et al. 1998) has been added. For clarity, the spectra are vertically shifted: a, b, c, d, e by +3500, +2500, +2000, +1500, +1000 cm^2/g, respectively.

Table 3. Annealing time and activation energy determined for glassy micrometre-sized $MgSiO_3$ particles using Eq. (1) and the constant $\nu_0 = 2 \times 10^{13}$ s^{-1}

Temperature (K)	Annealing time τ (min or h)	Activation energy E_a/k (K)
1121	3-5 min	40100-40700
1080	60-90 min	41900-42400
1060	150-190 min	42100-42400
1030	12-25 h	42540-43300
1000	>50 h	> 42700

Annealing experiments have been carried out at temperatures ranging from 1121 to 1000 K. In Fig. 3, the evolution of the mass absorption coefficient (MAC) has been monitored as a function of annealing time at 1121 K. Except the experiment at 1000 K, the $MgSiO_3$ glass was converted into orthoenstatite as could be verified by IR spectroscopy and XRD analysis. Crystallization has not been observed within 50 h at 1000 K in the IR spectrum, but weak indications of forsterite and tridymite formation have been found in the XRD spectrum.

Using Eq. (1) and $\nu_0 = 2 \times 10^{13}$ s^{-1}, the activation energy E_a has been calculated from the annealing times τ (see Table 3). It is evident that the values of E_a/k show a systematic decrease with growing annealing temperature. Therefore, Eq. (1) with the used value of ν_0 is not fully appropriate to describe the annealing process. We proved by plotting $\ln(\tau) = E_a/kT - \ln(\nu_0)$ that the exponential relation fits the measured data. However, the plot indicated that the value of the constant ν_0 has to be 4 to 8 orders of magnitude larger. From our limited number of experiments, we cannot determine the constant exactly. In addition, the constant probably depends on the chemical composition and has to be determined for each smoke/glass independently. For the sake of consistency to Lenzuni et al. (1995), in this paper, we will further use their value. However, so long as the constant ν_0 has not been determined experimentally, one should bear in

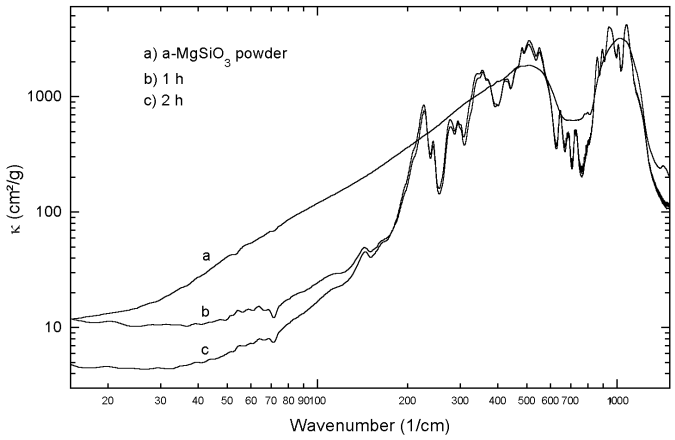

Fig. 4. Comparison of the IR spectrum of thermally untreated $\mathrm{MgSiO_3}$ glass powder (a) with the spectra of $\mathrm{MgSiO_3}$ glass powder that has been annealed at T=1121 K for 1 and 2 h (b, c).

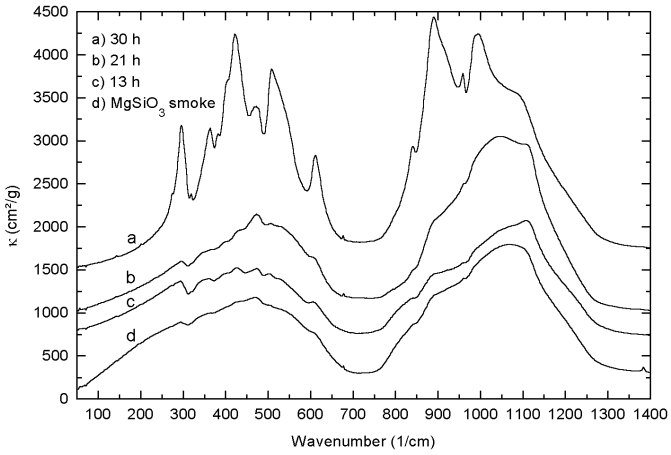

Fig. 5. Evolution of the MIR spectrum of $\mathrm{MgSiO_3}$ smoke after annealing at 1000 K up to 30 h. The annealing times are indicated. For clarity, the spectra are vertically shifted: a, b, c by +1500, +1000, +750 $\mathrm{cm^2/g}$, respectively.

mind that the numerical value of the activation energy depends on the estimation for ν_0.

The annealing times obtained for glass powder are compatible to the growth velocities that have been obtained from the bulk glass. For example, at 1080 K, the growth velocity was determined to be 72 nm/min. At this velocity, surface crystal growth would fully crystallize a particle of 5 μm in diametre in approximately 70 min. This is in the range of the annealing time measured for the glass particles. We conclude that the velocity of crystal growth does not depend on the particle size. In contrast, nucleation strongly depends on the surface area available and therefore determines the time-lag before crystal growth starts.

The opacity of untreated and annealed $\mathrm{MgSiO_3}$ powder has been obtained in the FIR range up to $15\,\mathrm{cm^{-1}}$. After 1 hour annealing at 1121 K, a distinct drop in opacity has occurred below 200 $\mathrm{cm^{-1}}$. An additional drop was observed in the wavenumber range $\nu < 100\,\mathrm{cm^{-1}}$ after 2 hours of annealing (see Fig. 4, spectra b and c).

Using Eq. (4), the spectral indices β of $\mathrm{MgSiO_3}$ powders have been estimated by least-square fits of the data in the range from 200 $\mathrm{cm^{-1}}$ to 50 $\mathrm{cm^{-1}}$. The parameters are $\beta = 1.50$ and $\kappa_0 = 0.115\,\mathrm{cm^2/g}$ for the untreated amorphous $\mathrm{MgSiO_3}$ powder. For the sample that was annealed at 1121 K for 2 hours, the parameters are $\beta = 1.36$ and $\kappa_0 = 0.028\,\mathrm{cm^2/g}$. As can be seen in Fig. 4, a further opacity drop occurs between 1 and 2 h of annealing. That drop may be caused by the continuous growth of the biggest crystalline regions that "consume" smaller nanocrystals. Another effect could be the "healing" of lattice defects in the nanocrystals.

4.2.2. Annealing of $\mathrm{MgSiO_3}$ smoke

The $\mathrm{MgSiO_3}$ smoke has been annealed at 1000 K to investigate the behaviour as a function of annealing time. Using IR spectroscopy and TEM, significant structural evolution of the smoke particles has not been observed prior to crystallization. In detail, TEM imaging showed that the texture with voids and rims was still preserved (see Fig. 1). Smoke evolution could not be characterized by a distinct stall phase as was observed by Hallenbeck et al. (1998). In contrast to the laser-ablated smoke described in this study, the Hallenbeck smoke was prepared at 770 K from Mg metal placed inside a furnace tube and a 1:1:4 flowing gas mixture of $\mathrm{SiH_4}$, $\mathrm{O_2}$ and He at a total pressure of 80 Torr. Although both laser-ablated smoke and smoke produced in a gas-flow-reactor are nonstoichiometric condensates, the latter is dominated by micrometre-sized entities of pure silica with a nanometre-sized mantle of chaotic Mg-silicate whereas our laser-ablated smoke consists of different-sized particles that are Mg-enriched or depleted according to their grain size. There is a basic compositional difference. For these reasons, both products cannot be compared with each other. That means that the stall phase need not be expected in all varieties of smoke particles.

Our results are shown in Fig. 5. The structure in the wide 10 μm profile of spectrum d indicates that some predominantly amorphous particles already contained forsterite microcrystallites. The main component at 1050–1100 $\mathrm{cm^{-1}}$ has been assigned to amorphous silica and the shoulder at 900 $\mathrm{cm^{-1}}$ to forsterite. The peaks of spectrum a in the 10 μm range at 843, 890, 960 and 1000 $\mathrm{cm^{-1}}$ can be identified with those of forsterite, whereas a shoulder at 1090 $\mathrm{cm^{-1}}$ has been assigned to amorphous silica.

As Fig. 5 demonstrates, rapid crystallization sets in not earlier then after 21 h of annealing. Therefore, the true annealing time used to calculate the activation energy has to be in the range between 21 and 30 h and is estimated to be $25 \pm 5\,\mathrm{h}$. Using Eq. (1) and the mean frequency $\nu_0 = 2.0 \times 10^{13}\,\mathrm{s^{-1}}$, the activation energy of the $\mathrm{MgSiO_3}$ smoke has been determined to be E_a/k = 42040 $\pm$ 150 K.

In the FIR, a significant opacity drop occurs between 250 and 75 $\mathrm{cm^{-1}}$. At 283 and 325 $\mathrm{cm^{-1}}$, tridymite features have been observed (see Fig. 6, spectrum b). Hence, the '30 h' smoke consisted of polycrystalline forsterite, tridymite and amorphous silica (see Fig. 6 and 9).

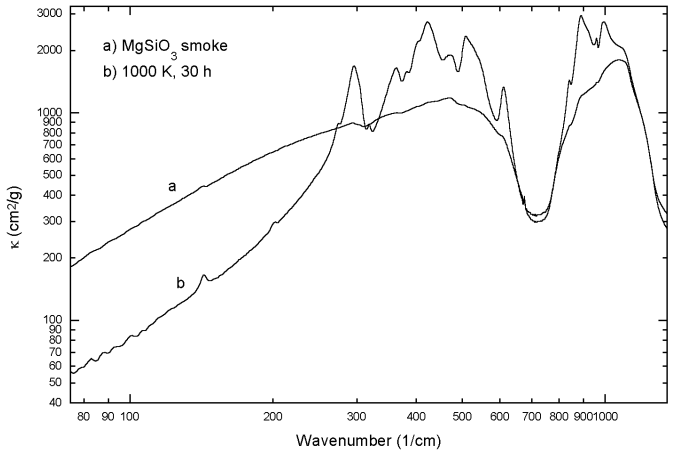

Fig. 6. Comparison of the IR spectrum of thermally untreated $\mathrm{MgSiO_3}$ smoke (a) with the spectrum of smoke that has been annealed at T=1000 K for 30 h (b).

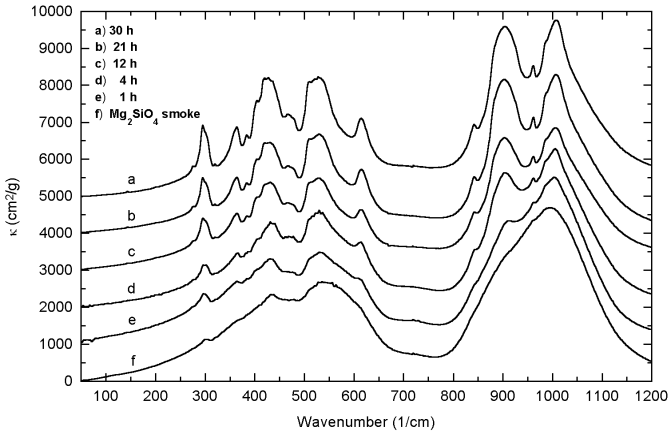

Fig. 7. Evolution of the MIR spectrum of $\mathrm{Mg_2SiO_4}$ smoke after annealing at 1000 K up to 30 h. The annealing times are indicated. For clarity, the spectra are vertically shifted: a, b, c, d, e by +5000, +4000, +3000, +2000, +1000 $\mathrm{cm^2/g}$, respectively.

Annealing experiments using laser ablated smoke from a natural pyroxene mineral were already carried out by Brucato et al. (1999). In contrast to our study, the peaks of the annealed samples fall nearly at the same positions as for the crystalline pyroxene, i.e. the smoke changed into crystalline pyroxene whereas our smoke transformed into forsterite and silica. Presumably, the presence of iron promotes pyroxene formation; but iron-free Mg-silicate smokes change into forsterite and silica. The activation energies given by Brucato et al. (1999) (47500 K) are not comparable to the ones determined here since they are based on a different definition of the annealing time. In contrast to the Lenzuni et al. (1995) perception, they define the anneling time, when the IR spectra do not change any longer, i.e. when the sample is crystallized completely.

4.2.3. Annealing of $\mathrm{Mg_2SiO_4}$ smoke

The $\mathrm{Mg_2SiO_4}$ smoke has been annealed at 1000 K up to 30 h and at 1206 K for 1 h. The results are presented in Figs. 7 and 8. The IR spectra proved the smoke to be converted into crystalline forsterite. The values of the MAC of annealed $\mathrm{Mg_2SiO_4}$ smoke coincide to the MAC of synthetic forsterite (Jäger et al. 1998). Because the smaller particle species had been magnesium deficient, some amorphous silica and MgO as well as crystalline $\mathrm{SiO_2}$ has to be contained in the smoke; but the weak amorphous features are superimposed by the strong crystalline peaks.

As can be seen in Fig. 7, the smoke starts to evolve significantly towards a polycrystalline material already after an annealing time of 1 h. From this spectra, we estimate the annealing time to be in the range between 1 and 2 h. Using Eq. (1) and the mean frequency $\nu_0 = 2.0 \times 10^{13}\,\mathrm{s^{-1}}$, the activation energy of the $\mathrm{Mg_2SiO_4}$ smoke has been determined to be E_a/k = 39100 $\pm$ 400 K.

In the FIR, a significant opacity drop occurs below 250 $\mathrm{cm^{-1}}$ (see Fig. 8). The overall opacity falls below that of the annealed $\mathrm{MgSiO_3}$ smoke. Due to the higher initial magnesium content, most of the smoke has been transformed into crystalline

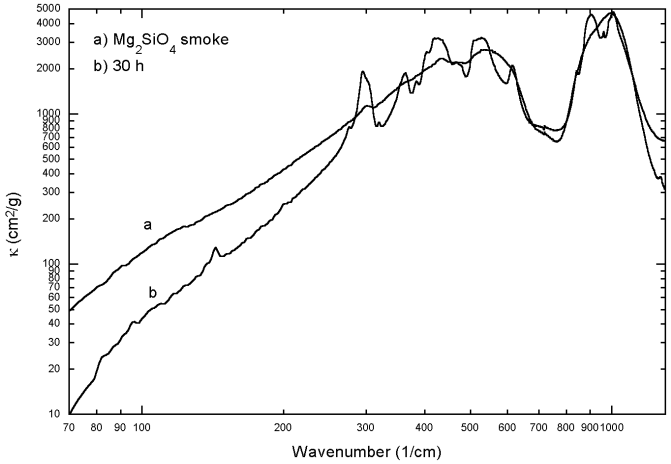

Fig. 8. Comparison of the IR spectrum of thermally untreated $\mathrm{Mg_2SiO_4}$ smoke (a) with the spectrum of smoke that has been annealed at T=1000 K for 30 h. (b)

forsterite. Otherwise, less amorphous silica and MgO is left that would significantly **raise** the FIR absorption.

4.2.4. Summary of $\mathrm{MgSiO_3}$ and $\mathrm{Mg_2SiO_4}$ smoke evolution

From our results, we conclude that the annealing of Mg-silicate smokes in oxygen-rich environments leads to polycrystalline c-$\mathrm{Mg_2SiO_4}$. If the Mg/Si-ratio falls below 2, the excess Si appears as tridymite and/or amorphous $\mathrm{SiO_2}$. The laser-ablated smoke had been rather inhomogeneous with two particle species, a small nanometre-sized fraction (10 to 50 nm in diametre, Mg-deficient) and a micrometre-sized fraction (0.1 to 2 μm in diametre, Mg-enriched). For these reasons, the presence of silica or crystalline $\mathrm{SiO_2}$ and MgO had to be expected even in the smoke of forsterite stoichiometry.

In the TEM, a profound difference between the annealing behaviour of the $\mathrm{MgSiO_3}$ and the $\mathrm{Mg_2SiO_4}$ smoke could not be observed. During annealing at 1000 K up to 30 h, the

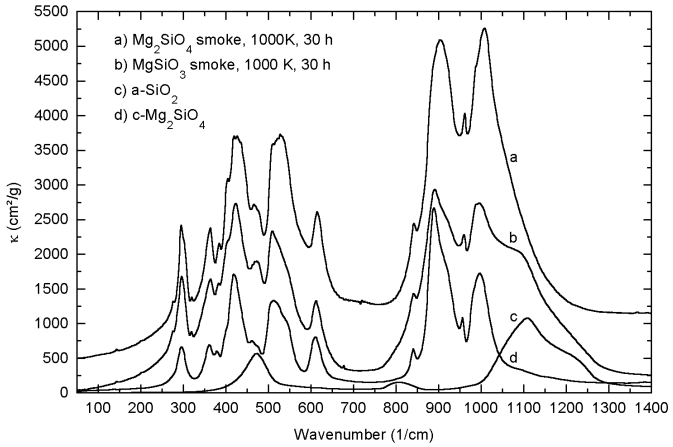

Fig. 9. The IR spectrum of annealed $\mathrm{Mg_2SiO_4}$ and $\mathrm{MgSiO_3}$ smoke (spectra a, b) compared with that of a-$\mathrm{SiO_2}$ (c) and c-$\mathrm{Mg_2SiO_4}$ (d) (Jäger et al. 1998). For clarity, spectra a is vertically shifted by $+500\,\mathrm{cm^2/g}$. The spectra c and d are in arbitrary units.

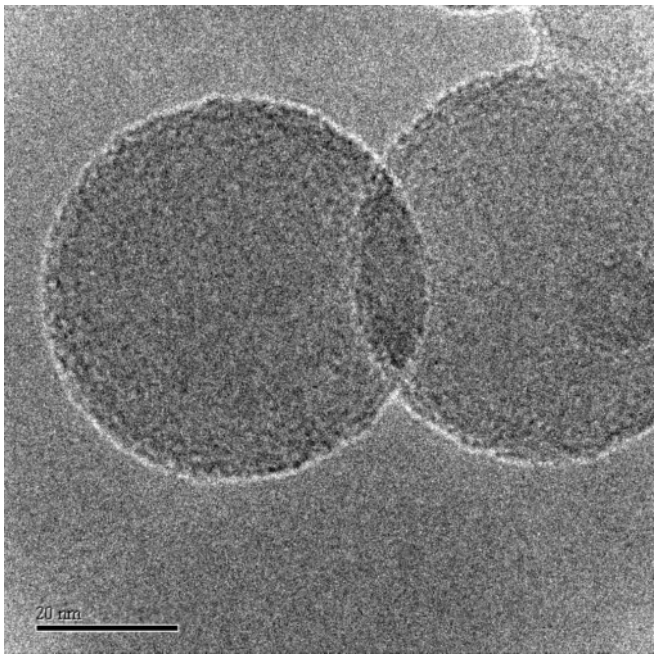

Fig. 10. TEM image of smaller-sized particles of the $\mathrm{Mg_2SiO_4}$ smoke after annealing up to 30 h at 1000 K. The Mg-poor particles that are characterized by a Mg/Si-ratio of about 1 seem to be structurally unchanged. However, they are partly crystalline as was checked by electron diffraction analyses.

smaller-sized smoke particles did not show observable changes. Although these Mg-poor particles seemed almost unchanged, electron diffraction analyses unvailed their partly crystalline structure. Hence, structural order has developed on a nanometre scale (see Fig. 10). These results are essentially the same for both the $\mathrm{MgSiO_3}$ and the $\mathrm{Mg_2SiO_4}$ smoke. The percentage of crystalline forsterite depends on the initial Mg/Si ratio of the particles that had been different for the $\mathrm{MgSiO_3}$ and the $\mathrm{Mg_2SiO_4}$ smoke. At 1206 K, nanocrystals have been observed showing that long range order has developed (see Fig. 11). The Mg-enriched micrometre-sized particles had been almost totally crystalline as was monitored by electron diffraction. Their outer appearance as sperical droplets did not change. According to their inital composition (Mg/Si ≈ 1 for the $\mathrm{MgSiO_3}$ smoke and 2 for the $\mathrm{Mg_2SiO_4}$ smoke), they most probably consisted of a mixture of crystalline forsterite and amorphous/crystalline silica or forsterite.

From the experiments, we found a significant decrease with increasing Mg/Si-ratio in the annealing time and therefore in the activation energy. For the $\mathrm{MgSiO_3}$ smoke, we found E_a/k = 42040 $\pm$ 150 K. For the $\mathrm{Mg_2SiO_4}$ smoke, E_a/k has been determined to be 39100 ± 400 K. Because of the Mg-deficiency in the $\mathrm{MgSiO_3}$ smoke, the diffusion rate of Mg-atoms limits the growth rate of the forsterite nanocrystals – increasing the macroscopically measured annealing time.

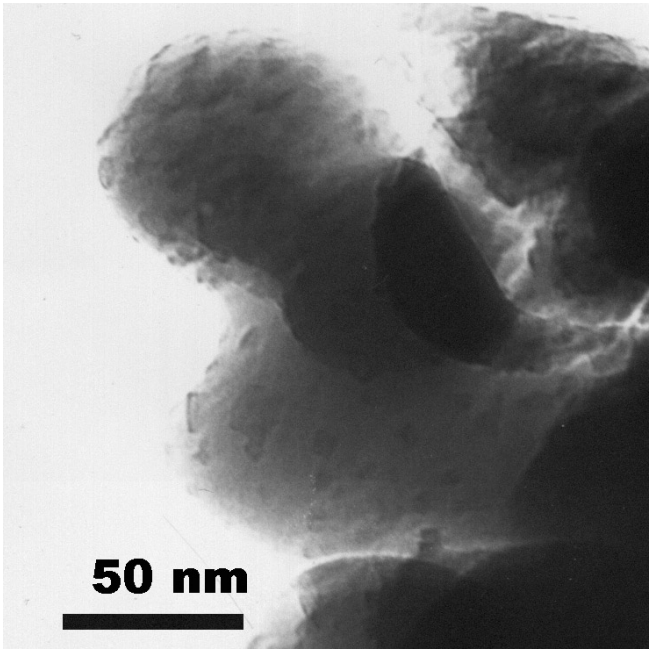

Fig. 11. TEM image of $\mathrm{Mg_2SiO_4}$ smoke that has been annealed at 1206 K for 1 h. Forsterite single crystals are embedded in a matrix made up of polycrystalline forsterite, crystalline and amorphous silica and MgO.

4.2.5. Annealing of amorphous silica nanoparticles

Amorphous silica is a primary condensate formed from MgO- or FeO-$\mathrm{SiO_2}$ vapour at non-equilibrium conditions (Rietmeijer et al. 1999).

To investigate the evolution of pure $\mathrm{SiO_2}$ condensates, nanoparticles of precipitated silica (commercial product, *Fisher Scientific Ltd.*) with diametres of 10 to 50 nm have been annealed at temperatures between 1150 and 1350 K. Their thermal evolution has been monitored by the appearance and the sharpening of the crystalline cristobalite and tridymite features in the infrared spectra (see Fig. 13 and 12). IR and XRD analysis proved cristobalite to be the major component. Peak positions and the

Table 4. Crystalline features in annealed silica (T = 'tridymite feature', C = 'cristobalite feature' (Hofmeister & Rose 1992, Nyquist 1997))

Peak position (cm^{-1})	FWHM of a-silica (cm^{-1})	FWHM of annealed silica (1220 K, 5 h) (cm^{-1})
1206 (T,C)	–	observed
1097 (T,C)	170 (shoulder at 1200)	$\approx$ 100 (shoulder at 1150 (T))
794 (T,C)	74	31 (peak sharpening)
624 (T,C)	–	13 (new peak)
472...488 (T,C)	60 (peak at 472)	55 (peak shifts to 488)
383 (T,C), 325 (T), 299 (T,C), 283 (T), 143 (C)	–	20...4 (new peaks)

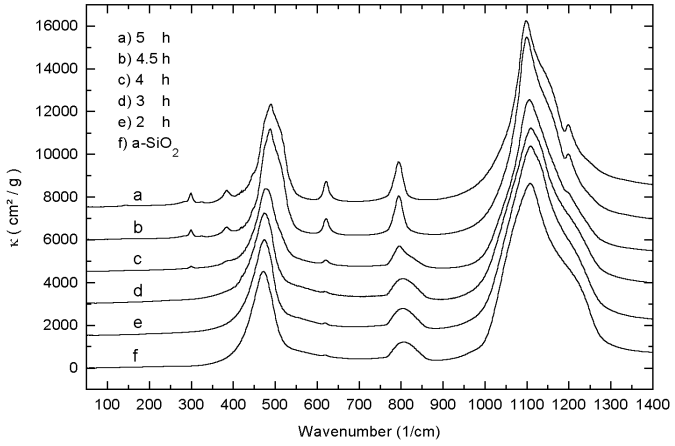

Fig. 12. Evolution of the MIR spectrum of silica that has been annealed at 1220 K. The annealing times are indicated. For clarity, the spectra have been shifted vertically: a, b, c, d, e by +7500, +6000, +4500, +3000, +2500 cm^2/g, respectively. τ has been approximated to 4.5 ± 0.5 h.

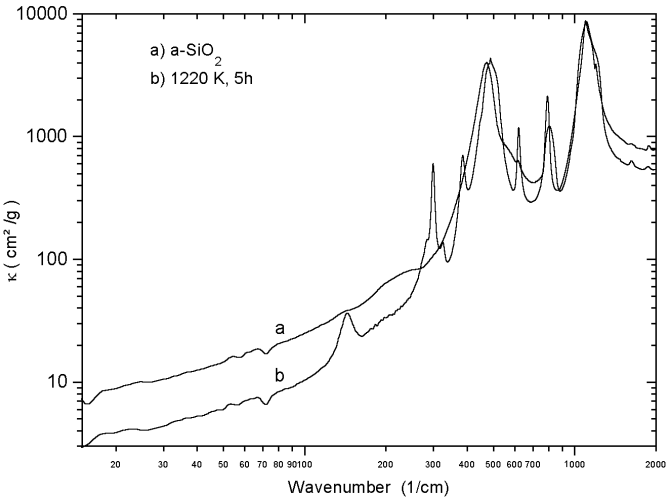

Fig. 13. Comparison of the IR spectrum of amorphous (a) with that of annealed silica (b) (T= 1220 K, 5 h).

full widths of half maximum (FWHM) of spectral features have been listed in Table 4.

At a temperature of 1220 K, the annealing time has been estimated to be 4.5 $\pm$ 0.5 h. Using Eq. (1) and $\nu_0 = 2.0 \times 10^{13}\,\mathrm{s}^{-1}$, the activation energy has been calculated to be E_a/k = 49190 $\pm$ 150 K. The diffusion constant D has been calculated as well (see Eq. (3))

$$D(T) = (4.2 \pm 0.8) \times 10^{-5} e^{\frac{49190}{T}} \frac{\mathrm{cm}^2}{\mathrm{s}}. \quad (5)$$

In Eq. (3), the constant a has been approximated to be 3.561 Å from the volume of the basic molecule forming the lattice ($M_\mathrm{mol} \times u/\rho = a^3$). $M_\mathrm{mol} = 60.085$ is the molecular weight of SiO_2, u the atomic mass unit and $\rho = 2.21\mathrm{g/cm}^3$ the mass density of a-SiO_2. Using the diffusion constant D and Eq. (2), the size of locally ordered structures can be estimated. At the annealing time of 4.5 h at 1220 K, it equals $\sqrt{2}a \approx 5$ Å. However, electron diffraction analyses showed that nanometre-sized crystals are present in the sample. Thus, the application of the formulas given in Sect. 3 is limited to the nucleation and should not be applied to the further growth of nanometre-sized crystals.

Crystallization of amorphous silica nanoparticles is associated with a sharpening of absorption features in the MIR and an opacity drop in the FIR (see Figs. 12 and 13). The mass absorption coefficient in the FIR has been approximated by a power law (using Eq. 4). The spectral indices β of silica have been estimated in the wavenumber range from 100 cm^{-1} to 15 cm^{-1}. For a-SiO_2, the parameters are $\beta = 0.64$ and $\kappa_0 = 1.20\,\mathrm{cm}^2/\mathrm{g}$. The parameters are $\beta = 0.62$ and $\kappa_0 = 0.55\,\mathrm{cm}^2/\mathrm{g}$ for the silica that has been annealed at 1220 K for 5 hours.

5. Discussion

Annealing experiments have revealed a significant distinction in the amorphous-to-crystalline transition between bulk and micrometre-sized glassy Mg-silicates on the one hand and nanometre-sized Mg-silicate smoke particles on the other hand. In detail, micrometre-sized particles and bulk sheets of glassy $MgSiO_3$ transformed into orthoenstatite whereas the $MgSiO_3$ and Mg_2SiO_4 smokes changed into forsterite, tridymite and amorphous silica. Weak indications of forsterite and tridymite formation in the $MgSiO_3$ glass powder have been observed in the XRD spectra only after annealing at 1000 K up to 50 hours. The timescale of crystallization of the silicate glass powder exceeds that of the smoke-like samples – showing the grain size dependence of heterogeneous nucleation.

At 1000 K, the smoke of $MgSiO_3$ composition changed from the amorphous state into forsterite in approximately one day. The excess SiO_2 appeared as crystalline tridymite and amorphous SiO_2. Because there had been a very Mg-deficient

small particle species, almost fully amorphous SiO_2 particles are still contained in the smoke.

Mg_2SiO_4 smoke has been found to evolve more quickly. At 1000 K, the annealing time was proved to be about 1 h. In contrast to the Mg-poorer $MgSiO_3$ smoke, the diffusion rate of Mg-atoms does not limit the growth rate of the nanocrystals because of the near forsterite stoichiometry of most of the particles. Amorphous and crystalline SiO_2 as well as MgO are also present in the smoke, because the smaller nanoparticles had been a Mg/Si-ratio below 2.

For amorphous SiO_2 nanoparticles, extrapolations proved the annealing time τ to surmount years at temperatures below 1000 K. At 1220 K, crystallization takes place after about 4.5 h. As was already noted above that might be true only for pure silica whereas Mg-silicates incline to tridymite formation.

Calculations of AGB star outflows showed that the temperature of silicate dust grains exceed 1000 K for mass losses higher than $\dot{M} \geq 3 \times 10^{-5} M_{\odot} \mathrm{yr}^{-1}$ (Sogawa & Kosaza 1999; Gail & Henning 1999). The outflowing gas decreases its temperature from the condensation point (maximum of the nucleation rate) in an outflow expanding with $v \approx 1 R_{\star} \mathrm{yr}^{-1}$ on the timescale of years (Sogawa & Kosaza 1999). Using the activation energy obtained for Mg_2SiO_4 smoke ($E_a/k = 39100$ K), the annealing times can be estimated for lower temperatures. Even at 800 K, homogeneous Mg_2SiO_4 nanoparticles are expected to develop a short-range order in about 3 yr. With decreasing Mg/Si-ratio, the activation energy and, therefore, the annealing times increase. Pure silica condensates with an activation energy of $E_a/k = 49190$ K may only at mass loss rates exceeding $\geq 3 \times 10^{-5} M_{\odot} \mathrm{yr}^{-1}$ develop an at least short range order. Silica may be a candidate to identify a feature at about 21 μm that recently has been observed in infrared spectra of evolved oxygen rich stars (Molster et al. 1999a).

6. Conclusions

As a result, rapid heating to temperatures exceeding 1100 K would be sufficient to recrystallize micrometre-sized glassy particles in a few minutes. In the history of the solar nebulae, a flash-heating event might have happened to the pre-chondrules. Because rapid cooling hindered complete crystallization, silicates both in the crystalline but also in the glassy state are observed in chondrules.

At a temperature of 1000 K, differently-sized amorphous magnesium silicates can be transformed into the polycrystalline state in the timescale of hours to days. According to the grain size and the kind of the amorphous material (smoke or glass), forsterite, tridymite and silica or enstatite have been formed. In detail, bulk and micrometre-sized $MgSiO_3$ glass evolved into orthoenstatite; nanometre-sized smokes changed into forsterite and silica.

For smoke-like nanoparticles, annealing times and activation energies have been determined (see Table 5). We found that E_a/k strongly depends on the Mg/Si ratio. It varies from 39100 K for Mg_2SiO_4 smoke and 42040 K for $MgSiO_3$ smoke to 49190 K for pure silica particles and determines the annealing times of the compositional different nanoparticles. For $MgSiO_3$ glass particles, a mean value of the activation energy could not be obtained. We indicated that the constant ν_0 that defines the value of E_a/k in Eq. (1) has most probably to be determined independently.

Table 5. Activation energies

Composition, structure	E_a/k (K)	Remarks
Mg_2SiO_4 smoke	39100	
$MgSiO_3$ smoke	42040	
$MgSiO_3$ glass	40100...43300	depending on T
SiO_2	49000	

7. Outlook

As a matter of fact, pure magnesium silicates have to be considered as a marginal case to real silicates. Annealing performance of silicates would be affected by the presence of iron, aluminium and less abundant elements (Karner & Rietmeijer 1996; Karner et al. 1996). Experiments using smoke containing iron and aluminium were already done by Brucato et al. (1999). They found that the smoke evolved into pyroxene – in contrast to this study.

Additionally, crystallization due to hydration has not yet been fully understood. Crystalline layer-lattice silicates observed in the cold dust component of the shell surrounding the young star HD 142527 may be formed by hydrocryogenic and low-temperature aqueous alteration or processes that can be described as low-temperature or athermal annealing (Malfait et al. 1999; Molster et al. 1999b).

More generally, formation of crystalline silicates by the process of annealing cannot be considered independently of dust-gas reactions. Far below the condensation temperature, amorphous silicates may undergo a change into hydrous crystalline silicates by equilibration with H_2O (Rietmeijer 1995).

Annealing is also responsible for chemical fractionation. Impurities (e.g. Al, Ca) may be released from the lattice and reassemble at the surface or in separate inclusions (Gail & Sedlmayr 1998). This effect would affect the spectroscopic properties of the silicate particles. At the present time, silicates that contain iron, calcium and aluminium as well as hydrous silicates are investigated and will be discussed in a succeeding paper.

Acknowledgements. This work was supported by the *Deutsche Forschungsgemeinschaft, DFG* project number Do 575/4–1 within the "Schwerpunktprogramm: Physik der Sternentstehung". We thank Gabriele Born for thoroughly doing the preparative work and A. Petrich (*Institut für Werkstofftechnik*, Jena, Germany) for helping to produce the laser-ablated smokes.

References

Bradley J.P., 1994, Science, 265, 925
Bradley J.P., Keller L.P., Snow T.P., et al., 1999a, Science 285, 1716
Bradley J.P., Snow T.P., Brownlee D.E., Hanner M.S., 1999b, In: d'Hendecourt L., Joblin C., Jones A. (eds.), Solid Interstellar Matter: The ISO Revolution, Springer-Verlag, Berlin. 298

Brearley J.A., 1996, In: Hewins R.H., Jones R.H., Scott E.R. (eds.), Chondrules and the Protoplanetary Disk, Cambridge University Press, Cambridge, 137
Brucato J.R., Colangeli L., Mennella V., et al., 1999, A&A 348, 1012
Crovisier J., Leech K., Bockelee-Morvan D., et al., 1997, Science 275, 1904
Dorschner J., Henning Th., 1995, A&AR 4, 271
Dorschner J., Begemann B., Henning Th., Jäger C., Mutschke H., 1995, A&A 300, 503
Frank W., Gösele U., Seeger A., 1979, In: Kekelidze G.P. (ed.), Radiation Physics of Semiconductors and Related Materials, Tbilisi State University Press, Tbilissi, 110
Gail H.P., 1998, A&A 332, 1099
Gail H.P., Henning Th., 1999, A&A, submitted
Gail H. P., Sedlmayr E., 1998, In: Hartquist T.W., Williams D.A. (eds.), The Molecular Astrophysics of Stars and Galaxies, Claredon Press, Oxford, 285
Gutzow I., Schmelzer J., 1995, The Vitreous State, Springer Verlag, Berlin
Hallenbeck S.L., Nuth J.A., Daukantas P.L., 1998, Icarus 131, 198
Hanner M.S., 1999, Space Science Rev., in press
Henning Th., 1999, In: d'Hendecourt L., Joblin C., Jones A. (eds.), Solid Interstellar Matter: The ISO Revolution, Springer-Verlag, Berlin, 247
Henning Th., Michel B., Stognienko R., 1995, Planet. Space Sci. 43, 1333
Hofmeister A.M., Rose T.P., 1992, J. Phys. Chem. 96, 10213
Jäger C., Mutschke H., Begemann B., et al., 1994, A&A 292, 641
Jäger C., Molster F.J., Dorschner J., et al., 1998, A&A 339, 904
Karner J.M, Rietmeijer F.J.M., 1996, LPS 27, 647
Karner J.M, Rietmeijer F.J.M., Janeczek J., 1996, Meteor. Planet. Science 31, A69
Koike C., Shibai H., Tuchiyama A., 1993, MNRAS 264, 654
Kojima T., Tomeoka K., 1996, Geochim. et Cosmochim. Acta 60, 14, 2651
Lenzuni P., Gail H.P., Henning Th., 1995, ApJ 447, 848
Malfait K., Waelkens C., Bouman J., de Koter A., Waters L.B.F.M., 1999, A&A 345, 181
Molster F.J. Waters L.B.F.M., van Loon J.Th., et al., 1998, Ap&SS 255, 469
Molster F.J., Waters L.B.F.M., Trams N., et al., 1999a, A&A 350, 163
Molster F.J., Yamamura I., Waters L.B.F.M., et al., 1999b, Nat 401, 6753, 563
Mutschke H., Begemann B., Dorschner J., et al., 1998, A&A 333, 188
Nuth J.A., 1996, In: Greenberg J.M. (ed.), The Cosmic Dust Connection, Kluwer Academic Publishers, Dordrecht, 205
Nyquist R.A., 1997, Infrared Spectra of Inorganic Compounds, Vol. 4, Academic Press, Inc., San Diego, 208
Rietmeijer F.J.M., 1995, LPS 26, 1163
Rietmeijer F.J.M., Nuth J.A., Mackinnon I.D.R., 1986, Icarus 66, 211
Rietmeijer F.J.M., Nuth J.A., Karner J.M., 1999, Phys. Chem. Chem. Phys. 1, 1511
Sandford S., 1996, Meteoritics & Planetary Science 31, 320
Scholze H., 1988, Glas, Springer Verlag, Berlin
Sogawa H., Kozasa T., 1999, ApJ 516, L33
Taylor S., 1992, Solar System Evolution, Cambridge Univ. Press, Cambridge
Thompson S.P., Evans A., Jones A.P., 1996, A&A 308, 309
Vogel W., 1985, Glass Chemistry, Springer Verlag, Berlin
Waelkens C., Malfait K., Waters L.B.F.M., 1998, Ap&SS 255, 25
Walters M.D., Boring J.W., Johnson R.E., Jesser W.A., 1988, Radiation Effects 106, 189
Waters L.B.F.M., Molster F.J., de Jong T., et al., 1996, A&A 315, L361
Wooden D.H., Harker D.E., Woodward C.E., et al., 1999, ApJ 517, 1034